Nuclear Materials and Energy 17 (2018) 217–221

Contents lists available at ScienceDirect

Nuclear Materials and Energy

journal homepage: www.elsevier.com/locate/nme

Analysis of the impurity flow velocity in a wide plasma parameter range for deuterium and hydrogen plasmas in the divertor legs of the stochastic layer in LHD

A. Kuzmin[a,*], M. Kobayashi[a], T. Nakano[b], G. Kawamura[a], M. Hasuo[c], K. Fujii[c], T. Morisaki[a], the LHD Experiment Group

[a] National Institute for Fusion Science, 322-6 Oroshi-cho, Toki, Gifu-ken 509-5292, Japan
[b] QST Naka Fusion Institute, 801-1 Mukoyama, Naka-shi, Ibaraki-ken 311-0193, Japan
[c] Kyoto University, Kyotodaigaku-katsura, Nishikyo-ku, Kyoto 615-8540, Japan

ARTICLE INFO

Keywords:
Spectroscopy
Hydrogen
Deuterium
Carbon
Impurity transport
Edge plasma

ABSTRACT

Impurity flow velocity measurements have been conducted for different magnetic field configurations in a wide plasma parameter range in the divertor leg region of LHD for understanding of the edge impurity transport. In all cases (densities, magnetic configurations, hydrogen (H) & deuterium (D) discharges), flows of several tens of km/s are observed. It is found that the flow in thick stochastic layer is faster than in thin stochastic layer configuration by a factor of 3. Different velocities of different charge states of carbon impurity are observed. The simulation with EMC3-EIRENE code shows similar trend as the experiments, but only qualitatively: faster flow in H compared to D discharges due to the mass effect, faster flow in the case of thick stochastic layer. However, synthetic spectra show discrepancy with experiments in the absolute Doppler shift, where the impurity velocity in the experiments is one order faster compared to the simulations.

1. Introduction

Understanding of the impurity transport in the edge plasma of fusion devices is essential to predict long range impurity migration, heat flux to the plasma-facing components and divertor performance [1]. The model for impurity transport in SOL used in numerical simulations has been compared with experimental observations [2,3,4,5], but still requires improvement and further validation of the transport model. For this purpose, one needs systematic measurements of impurity parameters such as flow and temperature, which can be compared with the numerical simulations based on the transport model.

In this paper, we present systematic measurements of impurity velocities of different ionization states of carbon (C^{+}–C^{3+}) in the divertor leg region in LHD. For these measurements an Echelle spectrometer is used [6]. Density dependence, isotope effect, and magnetic configuration effect are discussed based on the current impurity transport model. EMC3-EIRENE simulations of the impurity flow are made for different magnetic configurations and fueling gas. The comparisons of the experimental results with the simulations are discussed.

2. Experimental set-up and data selection

Typical discharge parameters of the data used in the present analysis are as follows. Toroidal magnetic field B_T = 2.75–2.53 T in counter-clockwise viewed from the top of the torus, three tangential neutral beams injected simultaneously with total power of 9–12 MW, line integrated electron density n_e = (1–14) × 10^{19} m^3, and the central electron temperature T_e = 1.5–3.5 keV. To study isotope effect on the impurity transport, hydrogen (H) and deuterium (D) discharges of the nineteenth cycle of LHD operation are used. The deuterium concentration C(D) = N(D)/(N(H) + N(D)), where N(H, D) is number of hydrogen or deuterium atoms in plasma, is C(D) = 0–0.25 in hydrogen discharges and C(D) = 0.75–1.0 in the deuterium discharges, respectively. The effect of the magnetic configuration on the impurity transport is studied in two different configurations. In the first one, the magnetic axis position is at R_{ax} = 3.6 m (Fig. 1(a)), in which the stochastic layer is thin. In the second one, R_{ax} = 3.90 m (Fig. 1(b)), in which the stochastic layer is thick. In Fig. 1 the color indicates the connection length of the magnetic field lines (L_C), and red color indicates flux tubes with $L_C > 10^5$ m, which corresponds to the confinement region. Yellow and green colors indicate the flux tubes inside the

* Corresponding author: National Institute for Fusion Science, 322-6 Oroshi-cho, Toki, Gifu 509-5292, Japan.
E-mail address: arseniy.a.kuzmin@gmail.com (A. Kuzmin).

https://doi.org/10.1016/j.nme.2018.11.009
Received 31 July 2018; Received in revised form 9 November 2018; Accepted 10 November 2018
Available online 26 November 2018

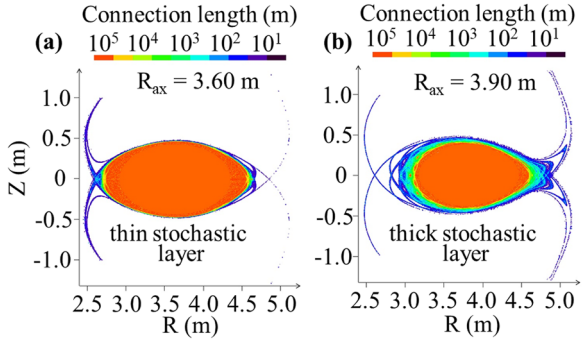

Fig. 1. Connection length distribution of the analyzed discharges. (a) Thin stochastic layer at R_{ax} = 3.60 m. (b) Thick stochastic layer at R_{ax} = 3.90 m. Color indicates connection length of magnetic field lines.

stochastic layer, which is noticeably thicker in the outward shifted magnetic configuration with R_{ax} = 3.90 m.

To measure the carbon impurity flow velocity in the divertor region of LHD, an Echelle spectrometer is used [6]. The same experimental set-up as in the previous work is kept. The spectrometer views the divertor leg from the outboard side, where the line of sight (LOS) is almost tangential to the magnetic field lines. The trajectory of the LOS mapped onto poloidal cross section of LHD plasma is shown below in Fig. 4. The following emission lines are used for analysis: C^+ (CII, $1s^2 2s2p3s–1s^2 2s2p3p$, 515.108 nm), C^{2+} (CIII, $1s^2 2s3s–1s^2 2s3p$, 464.742 nm), and C^{3+} (CIV, $1s^2 5f–1s^2 6g$, 465.751 nm $1s^2 5g–1s^2 6h$, 465.846 nm). The carbon flow velocities are calculated from the observed Doppler shift. The spectra are fitted with Gaussian function and the Doppler shift is calculated from the fitting results. The spectrometer is calibrated with the Th-Ar, Ne, Hg and He lamps. The XeI lines with wavelengths 467.1188 nm ($5p^5 6s\ ^2[3/2]^0–5p^5 7p\ ^2[5/2]$) and 462.4221 nm ($5p^5 6s\ ^2[3/2]^0–5p^5 7p\ ^2[3/2]$) are close to the analyzed CIII and CIV lines, and they are also used to confirm the wavelength calibration after the experiments. The error in the wavelength calibration is 4 km/s at maximum. An obvious Doppler shift of the analyzed lines is observed in experiments, as shown in Fig. 2, where CIII spectra are plotted for low and high density discharges.

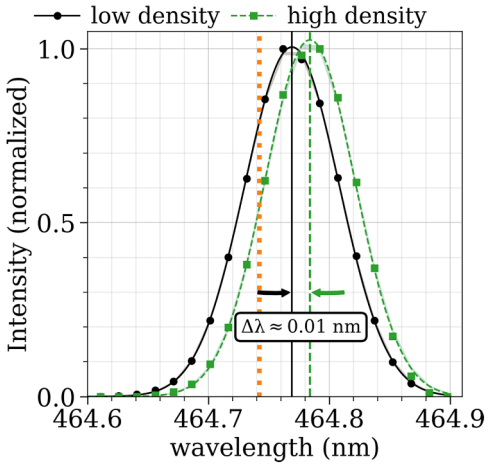

Fig. 2. An example of the Doppler shift of the CIII line in low ($\bar{n}_e$ = 2.4×10^{19} m^{-3}, #142449) and high ($\bar{n}_e$ = 6.1×10^{19} m^{-3}, #142441) density discharges. Dotted orange line indicates a non-shifted position of CIII line. The vertical black solid and green dashed lines represent the peak positions of the spectra of #142449 and #142441, respectively. The Doppler shift of ~ 0.01 nm is obvious in this comparison. (For interpretation of the references to color in this figure legend, the reader is referred to the web version of this article.)

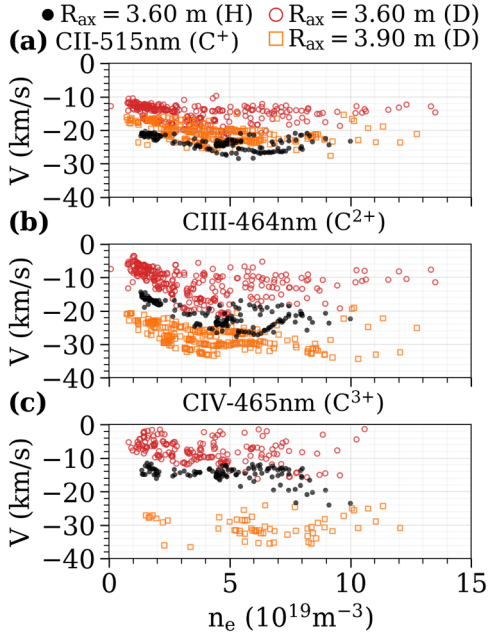

Fig. 3. Carbon impurity flow velocities of (a) C^+, (b) C^{2+}, and (c) C^{3+} ions. Open red circles – D plasma with R_{ax} = 3.60 m (thin stochastic layer). Black circles – H plasma with R_{ax} = 3.60 m (thin stochastic layer). Open orange squares – D plasma with R_{ax} = 3.90 m (thick stochastic layer). The data points with Gaussian fit errors smaller than 1 km/s are shown. (For interpretation of the references to color in this figure legend, the reader is referred to the web version of this article.)

3. Results

3.1. Experimental results

The experimental results are summarized in Fig. 3. The carbon impurity flow velocity is plotted against the line averaged electron density. Three cases are shown: thin stochastic layer (R_{ax} = 3.60 m) with D and H plasma, and a thick stochastic layer (R_{ax} = 3.90 m) with D plasma. The impurity flow in all configurations and for all densities are found to be negative, where the negative values mean flow away from the observation port. The meaning of positive and negative flow velocities are discussed in next section with transport simulations. It is found that impurity flow velocities for D plasma are systematically slower, by the factor of 1.4–2, compared to H plasma. This is considered due to mass effect of background plasma, $V_{\parallel} \propto \sqrt{1/m_i}$, which then affects the impurity velocity in H and D plasmas as discussed in ref. [6].

In D plasma of R_{ax} = 3.60 m (thin stochastic layer, the red open circles), the velocities of C^+ and C^{2+} are faster than that of C^{3+}. That is, for C^+ and C^{2+} the flow speed is in the range of 10–30 km/s, and in the range of 5–20 km/s for C^{3+} ions. In D plasma of R_{ax} = 3.90 m (thick stochastic layer, the orange open squares), the velocities between the different charge states changes. The velocities of C^+ are slower than that of C^{2+} and C^{3+}, where the flow speed is in the range of 15–25 km/s for C^+ ions and in the range of 25–35 km/s for C^{2+} and C^{3+} ions. The flow speed observed in the present experiments in LHD are in the same range or slightly faster than those observed in [4,7]. The velocities of C^{2+} and C^{3+} become faster in the outward shifted configurations. It is also noted that in the thick stochastic layer, impurity flow velocities are faster than in the thin stochastic layer by a factor of ~3. The impurity flow velocity increases moderately with increasing density in all cases. This density dependence is stronger especially for C^+ and C^{2+} ions. These systematic results of the impurity flow velocity are obtained for the first time in LHD, which are useful for further understanding of impurity transport in the stochastic layer and comparison with transport modeling.

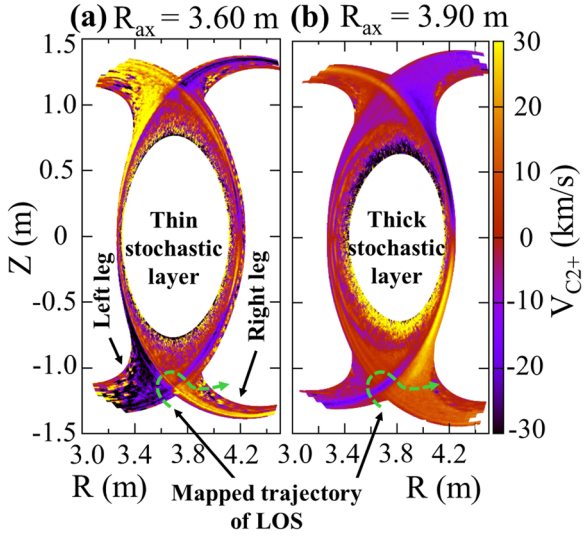

Fig. 4. Simulation results for the 2D distributions of parallel impurity velocity of C^{2+} (V_{C2+}) at vertically elongated cross section for (a) thin stochastic layer (R_{ax} = 3.60 m, #142441, P_{sol} = 10.4 MW, $n_{LCFS} = 5 \times 10^{19}$ m^{-3}) and (b) thick stochastic layer (R_{ax} = 3.90 m, #141682, P_{sol} = 9 MW, $n_{LCFS} = 4 \times 10^{19}$ m^{-3}). The mapped trajectory of LOS is shown by green lines. (For interpretation of the references to color in this figure legend, the reader is referred to the web version of this article.)

3.2. EMC3-EIRENE simulation

Fig. 4 shows 2D distribution of parallel flow velocity of C^{2+} in a vertically elongated cross section obtained by EMC3-EIRENE for R_{ax} = 3.60 m (Fig. 4(a), thin stochastic layer, #142441, P_{sol} = 10.4 MW, $n_{LCFS} = 5 \times 10^{19}$ m^{-3}) and 3.90 m (Fig. 4(b), thick stochastic layer, #141682, P_{sol} = 9 MW, $n_{LCFS} = 4 \times 10^{19}$ m^{-3}), respectively. In the simulations, the T_e and n_e profiles at the midplane are carefully matched to those in experiments obtained with Thomson scattering system by changing the cross field transport coefficients, $D_\perp$and $\chi_\perp$, as shown in Fig. 5. The match to T_e is rather good, while n_e has a certain deviation.

Shown with green lines in Fig. 4 are trajectories of the line of sight (LOS) of spectrometer mapped onto the cross section, where due to the helical rotation of the plasma against the LOS, the trajectories result in curved shape. The LOS enters plasma at the left divertor leg, goes into the stochastic region, and then comes out through the right divertor leg. The dark (blue) and the yellow (bright) colors represent the velocity in negative and positive directions in toroidal direction. Since the LOS views the plasma towards positive toroidal angle, the sign of the flow in Fig. 4 is the same direction as in Fig. 3. The flow velocity profiles along the LOS are plotted in Fig. 6 for the thin stochastic cases with hydrogen and deuterium discharges, where the contributions from each term in the parallel momentum balance of impurity transport [8] are also shown. As seen in Figs. 4 and 6, the flow directions of V_{C2+} change the sign along the LOS, i.e., negative values in the left legs at L = 3.0 ~ 3.5 m and positive values in the stochastic layer and at the right leg L = 3.5 ~ 4.7 m. The maximum values at the left leg are in the same order as the experimental values as observed in Fig. 3, ~ −20 km/s. It is found that in this density range, the flow speed is almost determined by the friction force, with small opposite contribution of the ion thermal force. The velocity in the deuterium case is slower than the hydrogen case, which is due to the effect of ion mass, m_i, where the background velocity is proportional to $\sqrt{(T_e + T_i)/m_i}$.

In order to directly compare the simulation results with experiments, synthetic spectra are constructed from the simulations as follows,

$$I(\lambda) = \sum_j \frac{i_j\, dl_j}{\sqrt{2\pi\sigma_{inst}^2}} \exp\left\{-\frac{(\lambda - \lambda_0 - \lambda_{shift})^2}{2\sigma_{inst}^2}\right\} \quad (1)$$

where i_j is emissivity of CIII (3 s ^{3}S–3p ^{3}P^o) in each cell j along LOS (W/m^3), which is obtained from photon emissivity coefficients in ADAS database [9] taking into account local T_e, n_e, and n_{c2+}. dl_j, σ_{inst}, and λ_0 are the distance of each cell j along LOS (m), instrumental width of the spectrometer at λ_0 (σ_{inst} = 0.023 nm), and the wavelength of the CIII emission (nm), respectively. The Doppler shift in the wavelength λ_{shift} is calculated as,

$$\lambda_{shift} = \lambda_0 \frac{1 - V_{C2+}\cos\theta\ /c}{\sqrt{1 - V_{C2+}^2/c^2}} \quad (2)$$

where θ is the angle between the tangent of field lines and the LOS (θ = 0 means the LOS is tangential to the field line), and c is the speed of light. The synthetic spectra are shown in Fig. 7 together with the experimental one. It is noted that the width of the spectra in simulations are slightly narrower than in the experiment, which is considered due to the broadening caused by finite impurity temperature and Zeeman splitting in the experiments, both of which are not included in the synthetic spectra obtained by the simulations. It is seen that the shift of the synthetic spectrum (black) is much smaller ($+4.4 \times 10^{-3}$ nm) than the experimental one (+0.042 nm), where the Doppler velocity from the synthetic spectrum is estimated at −2.8 km/s, while that in the experiment is −27 km/s. The small values in the simulation are due to

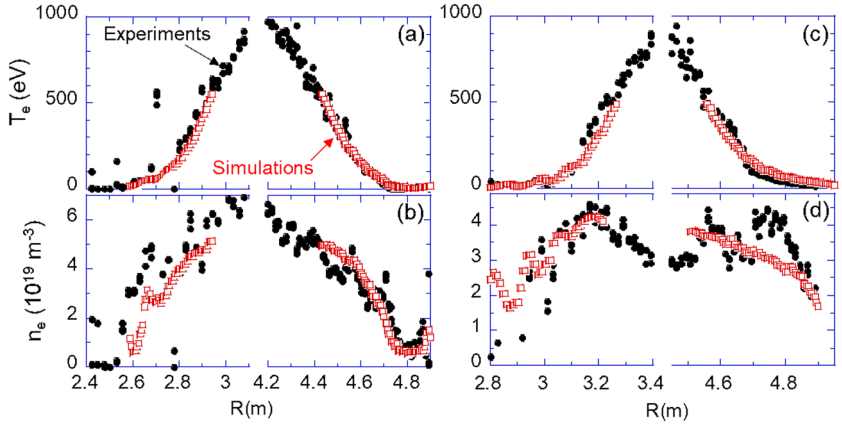

Fig. 5. Radial profiles of T_e and n_e. Black closed circles: experiments, red open squares: simulations, respectively. (a) and (b): thin stochastic layer (#142441, t = 4.0 sec, R_{ax} = 3.60 m). (c) and (d): thick stochastic layer (#141682, t = 4.7 sec, R_{ax} = 3.90 m). $D_\perp = \chi_\perp$ = 0.60 m^2/s for thin stochastic layer, and $D_\perp$ = 0.80, $\chi_\perp$ = 1.00 m^2/s for thick stochastic layer, respectively. (For interpretation of the references to color in this figure legend, the reader is referred to the web version of this article.)

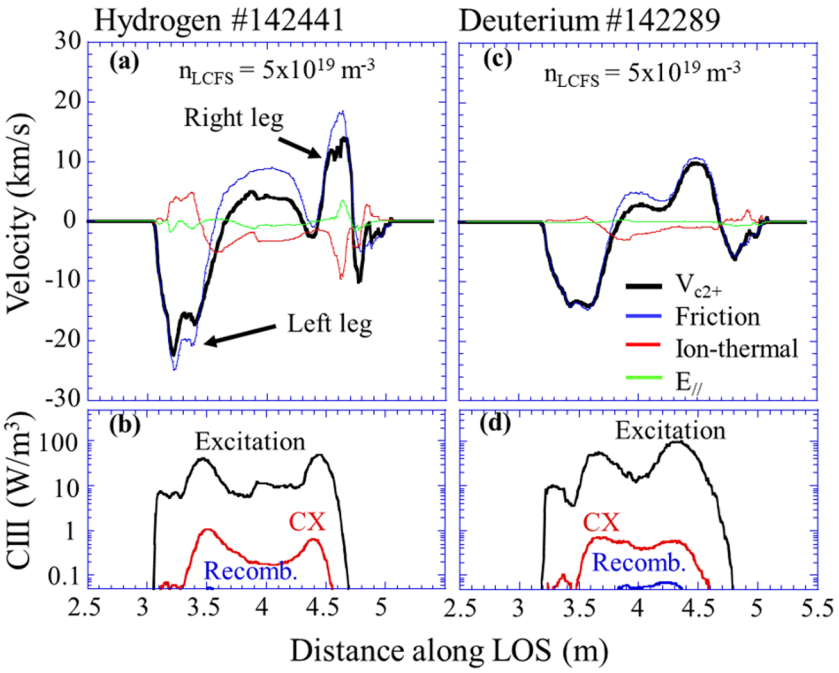

Fig. 6. Simulation results for the velocities and emission along LOS. (a) (c) Velocity and (b) (d) CIII emission profiles along LOS for the thin stochastic layer (R_{ax} = 3.60 m). (a) (b) in hydrogen case (same as in Fig. 4(a)), (c) (d) in deuterium case (#142289, P_{sol} = 10.8 MW, $n_{LCFS} = 5 \times 10^{19}$ m^{-3}). The CIII emissions are presented for excitation, recombining, and charge exchange components.

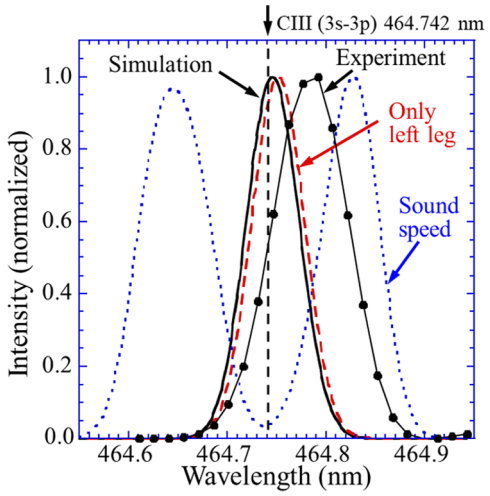

Fig. 7. Synthetic spectra reconstructed from simulations (black line) together with spectrum obtained in experiment (black line with closed symbols, #142441, t = 4.0 s). The red and blue lines show the synthetic spectra with integration only along left divertor legs and with sound speed instead of V_{C2+} in Eq. (2). (For interpretation of the references to color in this figure legend, the reader is referred to the web version of this article.)

the cancellation of the opposite flows in negative and positive directions along LOS, as shown in Fig. 6, when calculating the spectra with Eq. (1). The spectrum obtained by integration along only the left divertor leg is also shown in Fig. 7 with red dashed line, which has slightly larger Doppler shift resulting in −6.0 km/s. It is, however, still much smaller than the experimental value.

As shown in Fig. 6, the impurity ion is accelerated almost to the same level of background plasma ion (friction force contribution = background velocity) in this density range. The sound speed gives upper bound for the background velocity and thus for the impurity velocity, while the background plasma velocity is still far below the sound speed along the LOS. Just for comparison, the spectrum calculated from the local sound speed instead of V_{C2+} in Eq. (2) is plotted in Fig. 7. There appears a clear splitting in positive and negative sides, each of peaks is attributed to the left and right divertor legs, respectively. It is seen that the experimental spectrum is in-between the simulation with V_{C2+} and the sound speed.

The Doppler velocity obtained from the experiments and the simulations that have been converged by the time of writing this manuscript are summarized in Table 1 for different densities, magnetic configurations and hydrogen isotopes. The simulation results reproduce the tendency of the velocity change observed in the experiments qualitatively. There is, however, still a large discrepancy in the quantitative values, by an order of magnitude. In the simulations, the slower velocity in D than in H is due to the mass effect as mentioned above. The faster velocity in R_{ax} = 3.90 m (thick stochastic layer) is caused by larger emission at the left divertor leg than the right divertor leg. The positive velocity in the low density case ($n_{LCFS} = 2.0 \times 10^{19}$ m^{-3}) is caused by a strong thermal force that opposes to the friction force, resulting in the change of flow direction, where, however, the synthetic spectra becomes non-Gaussian. Such effect is not observed in the experiments.

Possible reason for the discrepancy is mismatch of the background plasma parameters in the divertor leg regions between the simulation and the experiments, which affects the velocity of background plasma and impurity, as well as the emission distribution. While the upstream profiles of T_e and n_e are matched to the experiments as described above, the downstream profiles can be different from the experiments as compared with the divertor probe measurements [10]. More systematic simulations including other charge states are ongoing and will be presented elsewhere.

Table 1
Summary of Doppler velocity of C^{2+} obtained in experiments and simulations.

	Experiments	Simulations
#142449 Thin stochastic layer (H) $n_{LCFS} = 2.0 \times 10^{19}$ m^{-3}	−18 km/s	+2.0 km/s
#142441 Thin stochastic layer (H) $n_{LCFS} = 5.0 \times 10^{19}$ m^{-3}	−27 km/s	−2.9 km/s
#142289 Thin stochastic layer (D) $n_{LCFS} = 5.0 \times 10^{19}$ m^{-3}	−18 km/s	−1.4 km/s
#141663 Thick stochastic layer (D) $n_{LCFS} = 5.4 \times 10^{19}$ m^{-3}	−27 km/s	−6.5 km/s

4. Summary

Impurity flow velocity measurements have been conducted for different magnetic field configurations in a wide plasma parameter range for H and D discharges at the divertor leg region in LHD for understanding of the edge impurity transport. In all cases (densities, magnetic configurations, H & D), large negatively directed flow, which corresponds to the divertor directed flow in the left divertor leg, is observed with several tens of km/s. At high densities, velocity in H discharges is faster than D by a factor of 1.4–2.0. Faster flow in H compared to D is considered due to the mass effect. Higher flow velocities are observed in the thick stochastic layer, by a factor of 3. Different velocities of different ionized states of carbon impurity are observed ranging from 5 to 35 km/s.

Impurity transport simulations with EMC3-EIRENE code have been conducted. Simulations show that the impurity ions are accelerated almost to the same speed as the background plasma ions. In order to compare the simulation results with the experiments, synthetic spectra are calculated. Very small Doppler shift results are due to the cancellation of the opposite flows in the left and right divertor legs after integration of the velocity distribution along LOS, weighted with the impurity emission. It is seen that the Doppler shift in the experiments is still below the upper bound of the possible shift caused by sound speed of background plasma obtained in the simulation. The simulation results show similar trend as the experiments on the density, isotope and magnetic configuration dependencies, but only qualitatively. There is, however, still a large discrepancy in the quantitative values, including the flow directions, by an order of magnitude. Further analysis with simulations of different charge states and other parameter ranges are ongoing.

Conflict of interest

The authors declare that they have no known competing financial interests or personal relationships that could have appeared to influence the work reported in this paper.

Acknowledgments

This work has been financially supported by JSPS KAKENHI grant number JP16H04622, and by the NIFS budget ULPP026, UFEX106, and KOAP031.

References

[1] M. Kobayashi, Nucl. Fusion 55 (2015) 104021.
[2] M. Kobayashi, S. Morita, C.F. Dong, Nucl. Fusion 53 (2013) 033011.
[3] S. Dai, M. Kobayashi, G. Kawamura, Nucl. Fusion 56 (2016) 06605.
[4] T. Oishi, S. Morita, et al., Nucl. Fusion 58 (2018) 016040.
[5] C.M. Samuell, G.D. Porter, W.H. Meyer, Phys. Plasmas 25 (2018) 056110.
[6] A. Kuzmin, M. Kobayashi, T. Nakano, et al., Plasma Fusion Res. 13 (2018) 3402058.
[7] C.M. Samuell, et al., Experimental Verification of Three-Dimensional Impurity Flows Due to Temperature-Driven Pressure Gradients, PSI, 2018.
[8] P.C. Stangeby, The Plasma Boundary of Magnetic Fusion Devices, IOP Publishing, 2000 section 6.
[9] http://open.adas.ac.uk/.
[10] M. Kobayashi, et al., Divertor power load distribution in LHD and comparison with EMC3-EIRENE, 23rd ITPA Meeting on SOL/Divertor Physics, 24-27 Oct, Naka, Japan, 2016.